BNL-215909-2020-JAAM

Preparation and Structural Characterization of ZrO2/CuOx/Cu(111) Inverse Model Catalysts

R. Shi, J. A. Rodriquez

To be published in "Journal of Physical Chemistry C"

April 2020

Chemistry Department

Brookhaven National Laboratory

U.S. Department of Energy

USDOE Office of Science (SC), Basic Energy Sciences (BES) (SC-22)

DISCLAIMER

Preparation and Structural Characterization of $ZrO_2/CuO_x/Cu(111)$ Inverse Model Catalysts

Rui Shi[1], Mausumi Mahapatra[2], Jindong Kang[1], Ivan Orozco[1], Sanjaya D. Senanayake[2],

José A. Rodriguez[1, 2,*]

[1] Department of Chemistry, SUNY at Stony Brook, Stony Brook, New York 11794, United States

[2] Chemistry Division, Brookhaven National Laboratory, Upton, New York 11973, United States

*Corresponding author: rodrigez@bnl.gov

Abstract

CO_2 hydrogenation to methanol is regarded as a promising reaction to catalytically convert a major greenhouse gas (CO_2) into a value-added product (methanol). In the current study, scanning tunneling microscopy (STM) and X-ray photoelectron spectroscopy (XPS) were applied to investigate the growth mode of low coverages (<0.2 ML) of ZrO_2 in an inverse $ZrO_2/CuO_x/Cu(111)$ system, which has the potential to achieve a high selectivity for a direct CO_2 to methanol transformation. It was found that the morphology of ZrO_2 was strongly affected by the preparation method. The $ZrO_2/CuO_x/Cu(111)$ model catalyst prepared by the oxidation at 600 K of Zr pre-deposited on Cu(111) exhibited substantial mixing of ZrO_2 and CuO_x. In contrast, the direct deposition of Zr under an O_2 ambient over $CuO_x/Cu(111)$ at 600 K produced small ZrO_2 islands (10-12 nm in size) with a two-dimensional structure (i.e. only one layer of ZrO_2). XPS studies indicate that both preparation methods lead to $ZrO_2/CuO_x/Cu(111)$ surfaces. The model catalyst prepared by the direct deposition of Zr in O_2 was annealed up to 700 K in ultra-high vacuum. Both STM and XPS results suggest no apparent change in ZrO_2, while CuO_x was reduced at such annealing conditions. The island size of 10-12 nm observed for ZrO_2 on Cu(111) is much smaller than island sizes seen for CeO_2 (30-50 nm) and ZnO (300-500 nm) on the same substrate, opening the possibility for unique chemical properties.

1. Introduction

The concentration of anthropogenic CO_2 is projected to increase dramatically by the end of the century, in part, due to the combustion of fossil fuels, which may create a severe impact on the global climate.[1,2] CO_2 is regarded as an alternative feedstock by recycling it into value-added chemicals such as methanol, higher hydrocarbons, and oxygenates, thus creating a carbon-neutral fuel cycle.[3,4] CO_2 hydrogenation to methanol is a promising approach because methanol itself is an excellent liquid fuel and can be blended with gasoline. Methanol can also be directly converted into valuable chemicals, such as ethylene following the MTO (methanol-to-olefins) process as a raw material.[5,6]

Cu-based catalysts show promising activity and selectivity for methanol synthesis reactions.[7–9] Several studies have illustrated the importance of the Cu-ZnO interface in industrial $Cu/ZnO/Al_2O_3$ catalysts. High activity is attributed to a synergy between the Zn oxide support and the Cu.[10–14] The results of high-resolution transmission electron microscopy (HR-TEM) have shown that the active phase of $Cu/ZnO/Al_2O_3$ catalysts exhibits an inverse ZnO/copper configuration with the noble metal partially covered by aggregates of zinc oxide.[12] Indeed, a very large increase in catalytic activity of Cu (111) was seen after the deposition of ZnO islands on this substrate.[13,14] In general, the deposition of oxide nanoparticles (ZnO, CeO_2, TiO_2) on Cu(111) produces very good catalysts for C1 chemistry (CO oxidation, forward and reverse water-gas shift reaction, methanol synthesis)[8,13,14] These results have led to a large interest on the performance of inverse oxide/metal catalysts.[8] ~~during CO_2 hydrogenation.~~ ZrO_2 has also been considered as an excellent component of catalysts for methanol synthesis due to its high stability under reducing or oxidizing conditions.[15–19,20-24] It appears that the ZrO_2-Cu interface can achieve

a higher selectivity for a direct $CO_2 \rightarrow CH_3OH$ transformation than the traditional ZnO-Cu interface.[21,24] Due to the enormous complexity of the catalytic process for methanol synthesis, the understanding of the roles of ZrO_2 remains unsolved.

Several studies point out that the synthesis of methanol from CO_2 over Cu/ZrO_2 catalysts is dependent on the ZrO_2 morphology.[15,20–22] Whichever ZrO_2 phase is the critical component for this reaction is still in debate. Some researchers suggest that the presence of tetragonal (t-)ZrO_2 promotes the methanol formation from CO_2,[15,22] while others claim that monoclinic (m-)ZrO_2 is more active in the methanol formation.[21] In general, the differences in the ZrO_2 structure can be attributed to the concentration of hydroxyl (OH) groups and therefore, different acidity of these structures.[15] However, amorphous (a-)ZrO_2 is also proposed to be a good option as support.[18,23] It has been shown that the oxidation of a Cu_7Zr_3 alloy can form a combination of amorphous ZrO_2 and Cu clusters which have an activity and selectivity comparable to Cu/ZrO_2 catalysts prepared by conventional coprecipitation.[23] The adsorption of methanol on a-ZrO_2 is reported to be weaker than that on m-ZrO_2, which may aid in the mitigation of further decomposition of the desired product and in turn, promote the selectivity towards methanol.[18,19] Furthermore, theoretical calculations have predicted that the $ZrO_x/Cu(111)$ inverse configuration formed by the reduction of $ZrO_2/CuO_x/Cu(111)$ is an excellent catalyst for the binding and hydrogenation of CO_2.[24]

Based on the good activity seen for inverse oxide/metal catalysts for CO_2 hydrogenation,[10,13,14,24] this current work is focused on the preparation of different $ZrO_2/CuO_x/Cu(111)$ systems for future studies on the role of ZrO_2 and the ZrO_2-Cu interface during methanol synthesis. With these model systems, the unique chemical and

physical properties of ZrO_2 nanostructures can be compared with bulk structures in a more straightforward manner.[25] Furthermore, experimental observations can be compared with the results of theoretical calculations where a very good catalytic performance is predicted[24] and with data reported for other Cu-ZrO_2 interfaces.[15-24] Herein, two different vapor deposition pathways were applied to investigate the growth modes of ZrO_2 on Cu(111). ~~: (1) Zr was vapor-deposited on Cu(111) at 300 K and then oxidized at 600 K in a 5 × 10^{-7} Torr oxygen ambient, and (2) Zr was vapor-deposited on pre-oxidized CuO_x/Cu(111) at 600 K in a 5 × 10^{-7} Torr oxygen ambient.~~ The as-prepared surfaces were characterized by scanning tunneling microscopy (STM) and X-ray photoelectron spectroscopy (XPS). The STM results reveal that the morphology of ZrO_2 is strongly influenced by the preparation method.

2. Experimental Methods

An Omicron STM chamber was used to obtain STM images, and a preparation chamber connected to the STM chamber was used for sample cleaning, annealing, and catalyst surface preparation by vapor deposition. A Cu(111) single crystal (Princeton Scientific Corp) was cleaned by repeated cycles of Ar^+ ion sputtering followed by annealing at 850 K. The Zr was vapor deposited using a commercial metal evaporator (Scienta Omicron). Two different vapor deposition pathways were applied to investigate the growth modes of ZrO_2 on Cu(111): (1) Zr was vapor-deposited on Cu(111) at 300 K and then oxidized at 600 K in a 5 × 10^{-7} Torr oxygen ambient, and (2) Zr was vapor-deposited on pre-oxidized CuO_x/Cu(111) at 600 K in a 5 × 10^{-7} Torr oxygen ambient. Deposition of Zr on pre-

oxidized CuO_x/Cu(111) without O_2 in the background led to oxygen deficient systems which have to be oxidized in order to get ZrO_2/CuOx/Cu(111). All STM images were obtained at room temperature, using a Pt-Ir tip.

XPS analysis was performed to follow the oxidation state of zirconium using a commercial SPECS chamber for Ambient-pressure X-ray photoelectron spectroscopy (AP-XPS) equipped with a PHOIBOS 150 EP MCD-9 analyzer (Mg Kα X-ray source) and a home-built XPS with a Scienta SES 100 spectrometer (Al Kα X-ray source), which are located at the Chemistry Division in Brookhaven National Laboratory. Zr was vapor-deposited on Cu(111) or pre-oxidized CuO_x/Cu(111) surface at the same condition as the STM samples. For the XPS spectra, Zr 3d, Cu 2p, O 1s, and C 1s regions were collected for each surface. The binding energies were calibrated by the position of Cu 2p. The Zr or ZrO_x coverage was determined by attenuation of the primary peak of the Cu substrate. The XPS spectra of the samples were collected under UHV (10^{-9} to 10^{-10} Torr) or under an O_2 pressure of $\sim 1 \times 10^{-6}$ Torr.

3. Results and Discussions

Here, two preparation methods for inverse ZrO_2/CuO_x/Cu(111) catalysts were adopted following our previously reported studies for ZnO/CuO_x/Cu(111).[26,27] In one of the methods, we start with bimetallic Zr/Cu systems as precursors for the mixed-metal oxide. This approach has been followed by many research groups when preparing inverse oxide/metal catalysts.[28,29] Following a second approach,[26–29] the Zr was vapor-deposited under a background of O_2 over a CuO_x/Cu(111) substrate. In the next two sections, the

influence of different preparation conditions on surface structure and composition will be discussed.

3.1 Oxidation of Zr/Cu(111) systems

A Zr/Cu(111) surface was prepared by vapor-depositing Zr metal onto a Cu(111) substrate at 300 K in UHV (1×10^{-9} Torr background). Figure 1(a-b) shows the STM images with different Zr coverages of 0.05 and 0.15 ML (monolayer). Under these preparation conditions, small Zr-related particles (2.0~2.5 Å in height, 5~10 nm in size) are randomly distributed on Cu(111). With the increase in coverage, as shown in Figure 1(b), most of the patches remain small in size, while some of them agglomerate into larger islands (more than 40 nm) as indicated by the white arrow. However, the growth of islands is in a two-dimensional (2D) pattern since the height of these islands remains the same (2.0~2.5 Å). XPS data to be discussed below showed that these features did not belong to Zr but to oxidized ZrO_x or $ZnOH_x$ species formed by reaction of the admetal with O-containing molecules present in the gas background of the chamber while dosing the zirconium.

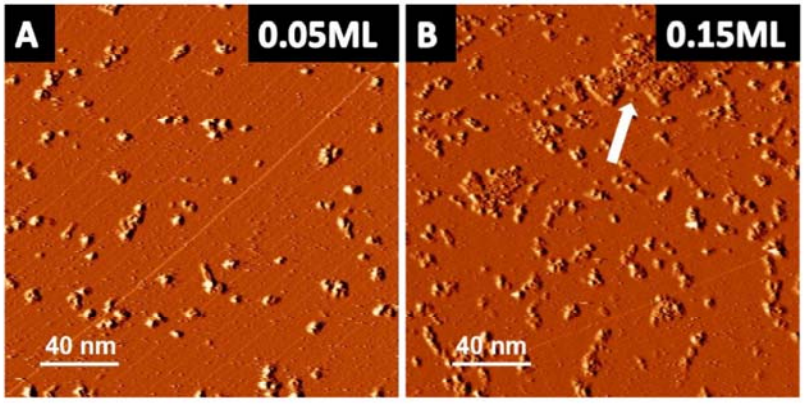

Figure 1. Series of STM dI/dV images (200×200 nm^2) after Zr was deposited onto Cu(111) at 300 K in UHV with different coverage: (a) 0.05 ML (V_t = -1.8 V, I_t = 0.06 nA),

and (b) 0.15 ML (V_t = -2.1 V, I_t = 0.06 nA). To get a better separation of the admetal and the substrate features, the images are shown in the current mode.

After the characterization mentioned above, the Zr/Cu(111) surfaces with different coverages (0.05 and 0.15 ML) were further oxidized at 600 K in a 5×10^{-7} Torr O_2 ambient for 20 minutes. Figure 2(a-b) shows the large scale STM images after the oxidation of the two Zr/Cu(111) surfaces. The small particles associated with zirconium in Figure 1, before full oxidation, can no longer be observed on both surfaces. Instead, large isolated islands form on the terraces of CuO_x after oxidation and the number of these islands increases with increasing Zr coverage as can be seen by comparing Figure 2(a) and 2(b) panels, which indicates a correlation between the initial presence of Zr and the formation of these islands, suggesting that they correspond to ZrO_2 or ZrO_2-CuO_x features. A zoomed-in STM image of such an island from Figure 2(a) is shown in Figure 2(c) and it clearly shows small CuO_x/Cu(111) domains of different orientations with typical CuO_x line structures separated by disordered structures. Similar formations can also be found elsewhere on the surface. As shown in Figure 2(d), a zoomed-in image of the terrace part in Figure 2(a) exhibits the well-ordered CuO_x "29" structure along with similar disordered structures indicated by the yellow circle.[30] The presence of such disordered structures forces the distortion of CuO_x structures instead of forming the typical long-ordered CuO_x structures under such oxidation conditions.[31] Therefore, those unidentified disordered structures are likely to be ZrO_2, which is incorporated within the CuO_x to form ZrO_2-CuO_x mixtures. The formation of ZrO_2-CuO_x islands was also due to the existence of ZrO_2, which delayed the nucleation and growth of CuO_x structures by limiting the diffusion of CuO_x precursors originating

from the Cu(111) step edges and terraces.[31,32] The same hindrance effect was also reported during the oxidation of Cu(100) in the presence of deposited Ag.[33]

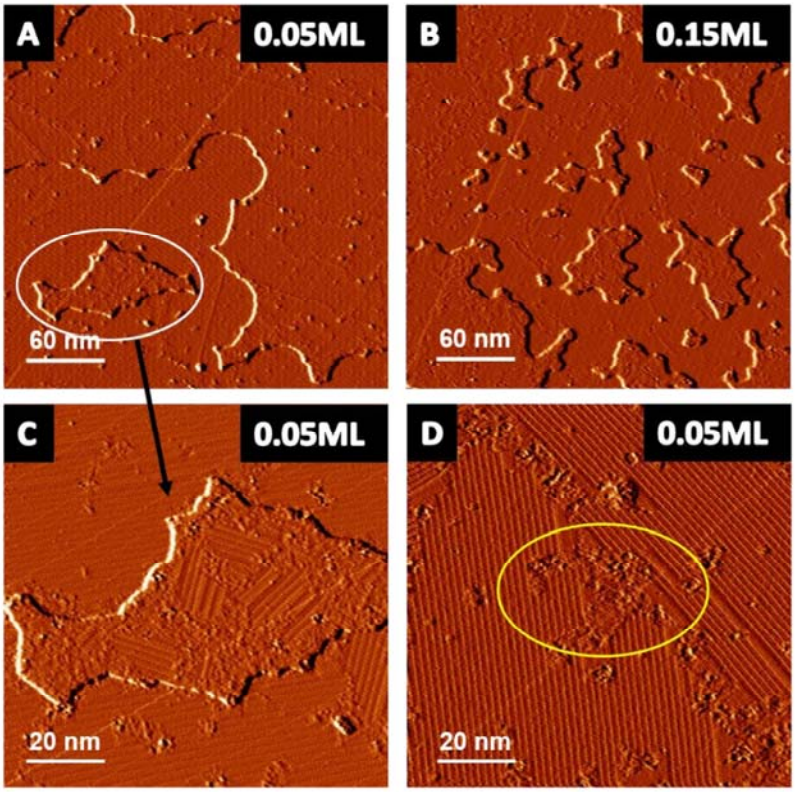

Figure 2. STM dI/dV images collected after the oxidation of Zr/Cu(111) surfaces (0.05 and 0.15 ML of Zr) at 600 K in 5×10^{-7} Torr O_2 for 20 minutes. (a) Oxidized 0.05 ML Zr/Cu(111) surface in a large scale (300×300 nm^2, Vt = -1.1 V, It = 0.10 nA), (b) Oxidized 0.15 ML Zr/Cu(111) surface in large scale (300×300 nm^2, V_t = -1.8 V, I_t = 0.10 nA), (c) A zoomed-in image of ZrO_2-CuO_x island from (a) (100×100 nm^2), and (d) A zoomed-in image of a terrace from the oxidized 0.05 ML Zr/Cu(111) surface. (100×100 nm^2). (c-d) were collected at V_t = -1.1 V, I_t = 0.10 nA tunneling conditions. To get a better separation of the admetal and the substrate features, the images are shown in the current mode.

The chemical state of the deposited Zr on Cu(111) and the oxidation process was followed using XPS. Figure 3 shows a series of Zr 3d (left) and O 1s (right) XPS spectra for a surface with 0.2 ML of zirconium. The Zr 3d doublet peaks with binding energies of ~182.4 ($3d_{5/2}$) and ~184.7 eV ($3d_{3/2}$) for the as-prepared sample (Figure 3, left, "As prepared" label) correspond to Zr^{4+} (ZrO_2).[34] Given the condition that Zr metal was deposited under UHV and without an O_2 ambient (background pressure of 1 x 10^{-9} Torr), this can be explained by the fact that Zr nanoparticles have a very high oxygen affinity so that they would scavenge all of the oxygenated residual gases in the chamber background during the timescale of the deposition (~20 min).[35] The O 1s XPS spectrum for the as-prepared sample (Figure 3, right, "As prepared" label) also shows a minor peak at ~530.5eV which proves that the deposition of Zr metal introduces oxygen species onto the surface, compared to the O 1s spectra for the Cu(111) surface before deposition (Figure 3, right, "clean Cu(111)" label). We always observed this behavior when small coverages of zirconium (≤ 0.2 ML) were deposited on Cu(111). The studies of zirconium surfaces on Cu(111) performed by Paulidou *et al.,* where metallic Zr was confirmed by XPS after depositing more than 2 ML of Zr metal on Cu(111) in UHV,[35] disagree with our low coverage case for the Zr/Cu system. However, considering the lack of oxidant gases in the chamber background together with more than 2 ML of Zr in the previous study,[35] their conclusion that most of the Zr species are in metallic form is reasonable. In our system, the Zr coverage is less than 0.2 ML, and the dominant Zr species is found to be ZrO_2(4+). However, according to the shape of the "valley" at ~183eV in the Zr 3d spectrum after deposition (Figure 3, left, "As prepared" label), it is possible that there may be overlapping species, such as $Zr(OH)_4$ or Zr(3+).[36] Due to the limited resolution of the lab-based XPS,

the concentration of different species cannot be quantitatively assigned. Therefore, in the following content, Zr-related structures by UHV deposition will be referred as Zr(4+) species, which may suggest a combination of oxides and hydroxides.

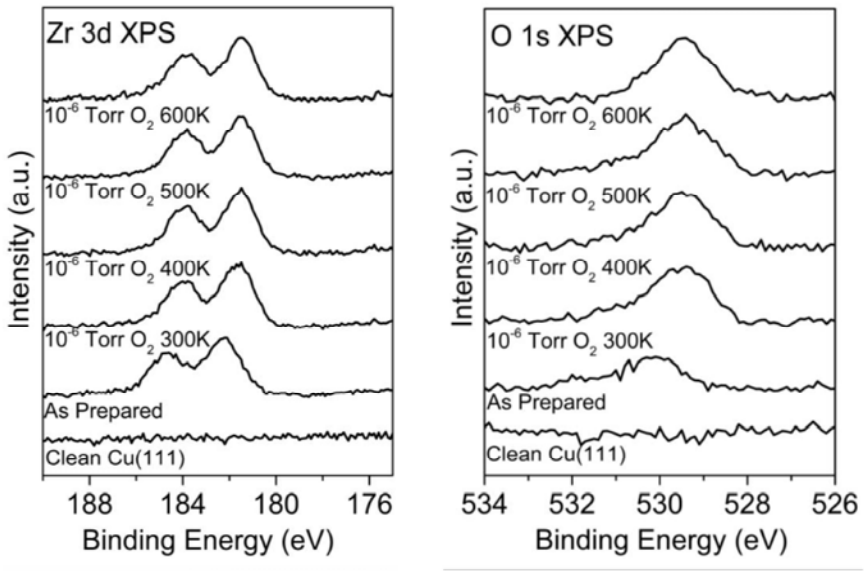

Figure 3. Zr 3d (left) and O 1s (right) XPS spectra for as-deposited Zr/Cu(111) at 300 K and $ZrO_2/CuO_x/Cu(111)$ by subsequent oxidation at elevated temperatures: 300, 400, 500 and 600 K in 1×10^{-6} Torr O_2

For the oxidation process of the Zr(4+)/Cu(111) surface, as shown in Figure 3, the Zr 3d XPS spectra (left) were collected at elevated temperatures from 300 to 600 K under a 1×10^{-6} Torr O_2 ambient. Fitting the Zr 3d data (Figure S1 in Supporting Information) using an asymmetric lineshape (Doniach-Sunjich) and constraining the peaks ($3d_{5/2}$ and $3d_{3/2}$) to both an identical full width at half the maximum (FWHM) and proper area ratio (2:3) resulted in peak narrowing under oxygen exposure (FWHM = 1.70 eV to 1.51 ± 0.02 eV)

due to a convergence of oxidation states present in the Zr (i.e. from trace amounts of Zr^{3+} to completely Zr^{4+}), allowing for a qualitative identification of Zr species present. Surprisingly, the Zr 3d peaks shifted to lower binding energies with the increasing oxidation temperature {~181.5 eV ($3d_{5/2}$) and ~183.8 eV ($3d_{3/2}$)}, which may indicate that the Zr cations are partially "reduced" under oxidation conditions. However, according to the O 1s spectra in Figure 3(right), the growth of O peak from CuO_x (~529.4eV) proves that the decrease in binding energy of Zr 3d spectra cannot be interpreted by only considering the change of oxidation state because Zr has a much higher formation enthalpy with oxygen (-1097.5 kJ/mol) compared to that of Cu (-170.7 kJ/mol).[37] A similar phenomenon was also observed in other studies, in which Ti_3O_5 clusters were deposited on Cu(111) and CuO_x/Cu(111).[38] It was found that for Ti_3O_5 clusters on CuO_x/Cu(111), the Ti 2p shifted to lower energies compared to Ti_3O_5 on the bare Cu(111) surface, which was explained by the uncompensated changes in the local work functions after the shift from Cu(111) to CuO_x/Cu(111) and also by possible final state effects. In addition, an XPS study on ZrO_2/Pt(111) also observed that under an oxygen ambient, the Zr 3d peaks shifted to slightly lower binding energies because of the presence of adsorbed oxygen on Pt(111).[39] Therefore, the shift of Zr 3d to lower binding energies has a high correlation with a change in the Cu substrate instead of the reduction of Zr cations.

3.2 Zr Deposition on CuO_x/Cu(111) at 600 K in a molecular oxygen background

According to our previous research on the preparation of the ZnO/CuO_x/Cu(111) model catalysts for CO_2 hydrogenation, Zn deposited on CuO_x/Cu(111) in the ambient of O_2 at 600 K exhibited a better thermal stability under typical reaction temperatures (550-600 K).[26] Therefore, in the second preparation method, the same methodology was applied to

generate the $ZrO_2/CuO_x/Cu(111)$ model catalyst. Cu(111) was first heated to 600 K with an exposure of 5×10^{-7} Torr O_2 for 15 minutes to make a well-ordered $CuO_x/Cu(111)$ surface as reported previously.[30–32] This $CuO_x/Cu(111)$ system had a characteristic O 1s binding energy of 529. eV.[40] The temperature of the $CuO_x/Cu(111)$ surface was maintained at 600 K, and Zr was deposited in a background of O_2 (5×10^{-7} Torr). In XPS, Figure 4, we observed the expected position for ZrO_2 on $CuO_x/Cu(111)$ in the Zr 3d region and a broad O 1s feature which indicates O signal coming from ZrO_2 and CuO_x oxides. The binding energies for Zr 3d are {~181.5 eV ($3d_{5/2}$) and ~183.8 eV ($3d_{3/2}$)}, which matches the position for $ZrO_2/CuO_x/Cu(111)$ model after the oxidation of Zr/Cu(111) system mentioned above. Besides the O1s signal from CuO_x (529.3eV, FWHM = 1.57eV), a new O1s peak was resolved after the deposition of ZrO_2 (529.9eV, FWHM = 1.67eV) and it's attributed to the O from ZrO_2 (fitting parameters are shown in Table S1, Supporting Information). Figure 5(a) shows a large scale STM image under these preparation conditions, where two distinct features can be observed on the $CuO_x/Cu(111)$ surface. The first feature in Figure 5(a) is assigned as ZrO_2 islands (labelled by yellow circles). A smaller-scale image of a selected island is shown in Figure 5(b) with an average size of ~10 nm and an average height of ~3 Å. It has been recently reported that one layer of ZrO_2 thin film grown on Pt(111), Rh(111) and Ru(0001) is around 3 Å.[39,41] Therefore, the ZrO_2 islands obtained by this method appear to be only one layer of ZrO_2 and no growth of further layers is observed at this coverage. The second feature noted on the $CuO_x/Cu(111)$ surface were small dots (labelled as "O_{ads}") of nearly identical size as indicated by the white circle in Figure 5(a). A zoomed-in image of the small dots is shown in Figure 5(c). When obtaining the STM images with smaller scales, these small dots were not stable on the

surface, which points to a high degree of mobility. In addition, depressions can be found in each small dot, as shown in the line profile of one of the dots, which are believed to be non-metallic adsorbates since the local density of states (LDOS) of the adsorbed site would be a minimum.[32,42] The apparent depth of the depression in the center of the small dot is ~0.5 Å, which matches a previous report for O adatom on Cu(111).[32] The formation of adsorbed O might be related to our preparation method in that the O_2 ambient was still maintained after deposition and during the cooling of the surface.

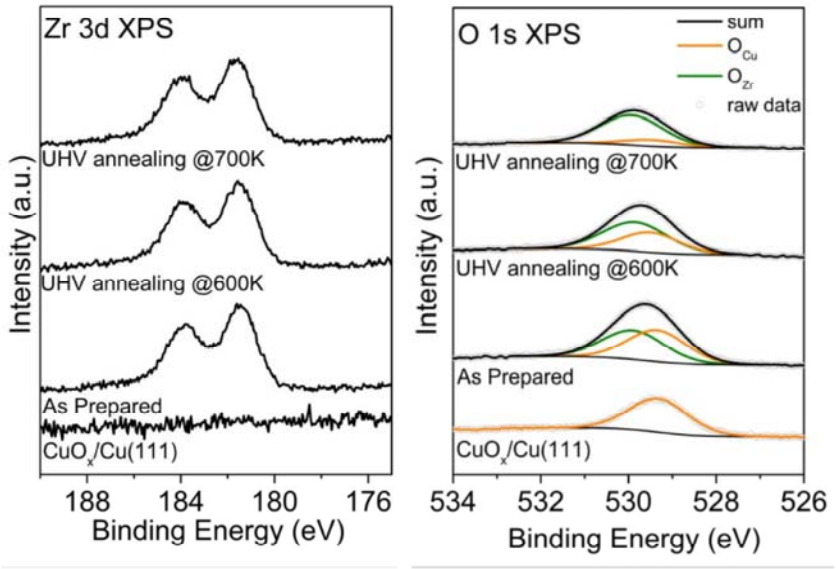

Figure 4. Zr 3d (left) and O 1s (right) XPS spectra for a $ZrO_2/CuO_x/Cu(111)$ surface prepared by deposition of Zr at 600 K under 5×10^{-7} Torr of O_2. The spectra after annealing the surface at 600 and 700 K in UHV were also collected.

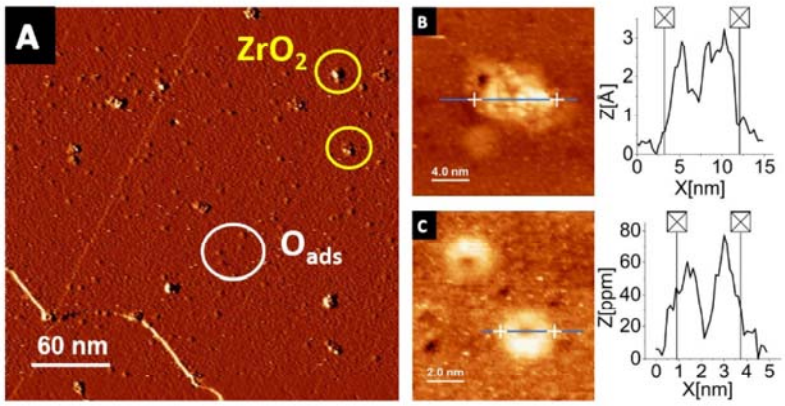

Figure 5. STM images after Zr was vapor-deposited on CuO_x/Cu(111) at 600 K in an atmosphere of 5×10^{-7} Torr O_2. (a) The ZrO_2/CuO_x/Cu(111) surface (0.02 ML) after the deposition (300×300 nm^2) is shown in derivative mode, (b) a smaller scale image of a selected ZrO_2 island and its line profile (20×20 nm^2), and (c) a smaller scale image of adsorbed O atoms and the line profile (10×10 nm^2). All the images were collected at V_t = -1.5 V, I_t = 0.10 nA tunneling conditions.

The thermal stability of this ZrO_2/CuO_x/Cu(111) surface was also investigated by annealing the sample up to 700 K in UHV. Firstly, it was annealed in UHV at 600 K for 15 minutes. XPS showed that this can induce the reduction of plain CuO_x/Cu(111) (Figure S2, Supporting Information). As shown in Figure 6(a), one noticeable change is clearly seen for the CuO_x/Cu(111) substrate in that some line defects of CuO_x were observed after annealing to 600 K, as indicated by the white arrow. The morphology of ZrO_2 islands was not affected by this annealing, and the average size and height of the islands remained around 10 nm and 3 Å, respectively. The surface was further annealed in UHV at 700 K for 15 minutes (Figure 6(b)). A larger area of defects can be observed on CuO_x/Cu(111) with the increasing annealing temperature, as indicated by the white arrow. No adatoms of

O can be resolved on the CuO_x/Cu(111) anymore, which suggests the desorption of O adsorbates under such annealing conditions. The size of the ZrO_2 islands remained around 10 nm; however, the apparent height was lowered to ~1.5 Å (Figure 6(c)), which might be related to the reduction of the CuO_x underneath the ZrO_2 islands, since no change in the ZrO_2 oxidation state was observed during the annealing process as suggested by the Zr 3d XPS spectra in Figure 4 (left). The O 1s XPS spectra (right) also indicate no reduction of O_{Zr} signal (~529.9eV) after annealing up to 700 K, while the O_{Cu} signal (529.4eV) decreased with elevated annealing temperature. This corroborates the STM images which show the reduction of CuO_x lines. The same annealing experiment was conducted on bare CuO_x/Cu(111) at 600K, the reduction of the CuO_x/Cu(111) is nearly complete at such temperature according to the O 1s XPS spectra (Figure S2, Supporting Information), while system with ZrO_2 still presents a small peak of CuOx from the O 1s XPS spectra (Figure 4). Therefore, ZrO_2 may have an ability to reserve CuO_x at lower annealing temperatures like 600K.

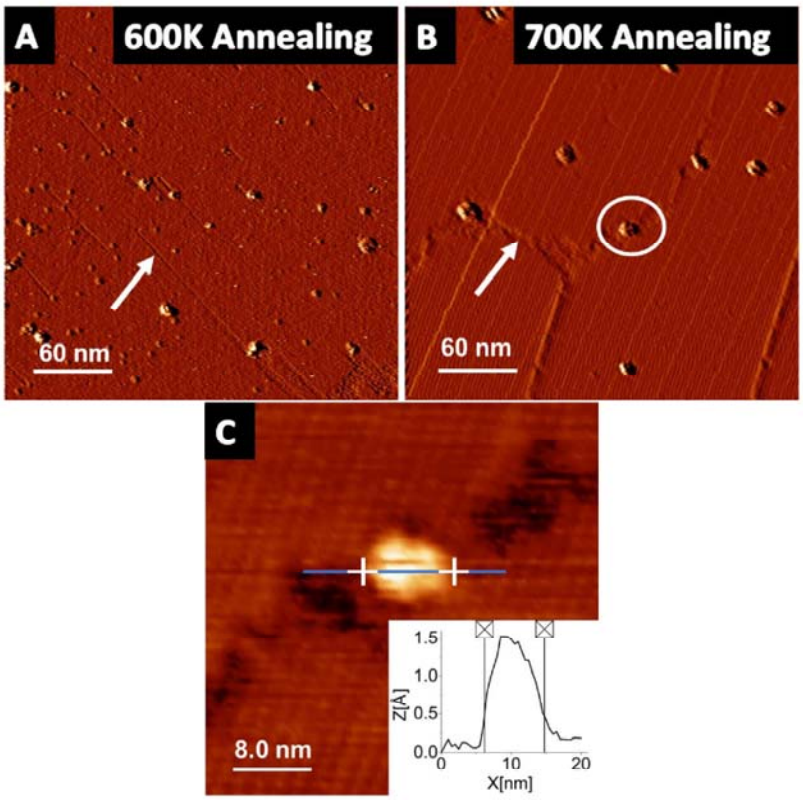

Figure 6. STM images of $ZrO_2/CuO_x/Cu(111)$ surfaces (0.02 ML) after annealing at 600 and 700 K in UHV. All the images were obtained at room temperature: (a) Annealed at 600 K in UHV for 15 minutes, (300×300 nm^2), shown in derivative mode, (b) annealed at 700 K in UHV for 15 minutes, (300×300 nm^2), in derivative mode, (c) a smaller scale image of a selected ZrO_2 island from (b) and its line profile (40×40 nm^2). All images were collected at V_t = -1.2 V, I_t = 0.10 nA tunneling conditions.

In previous studies, overlayers of ZrO_2 have been prepared on Pt(111), Rh(111) and Ru(0001).[39,41] These ZrO_2-metal interfaces can be useful for CO_2 hydrogenation. The ZrO_2-copper interface has the advantage of involving a metal with a low cost. Furthermore, the $ZrO_x/Cu(111)$ system has displayed good catalytic activity for CO_2 hydrogenation in

theoretical calculations.[24] Under the reducing conditions of CO_2 hydrogenation, any O bound to Cu(111), Pt(111), Rh(111) or Ru(0001) would be removed leaving only ZrO_2 on top of the metal substrate.[14,26] Pt, Rh and Ru can attack the CO formed by the decomposition of CO_2 to yield surface carbon trough the Boudouard reaction ($2CO \rightarrow C + CO_2$). The deposited C eventually would lead to deactivation and poisoning of the catalysts. This negative phenomenon would not be seen in the ZrO_2/Cu systems because copper does not dissociate CO. Thus, for the ZrO_2/Cu(111) catalysts, one can expect a low cost, high activity[24] and large stability.

Cu(111) has been used as a substrate for the generation of inverse CeO_2/Cu(111) and ZnO/Cu(111) catalysts.[13,14,26,43] Ce and Zn atoms react with Cu(111) forming metallic alloys which do not show an easy reaction with O-containing molecules present in the background of UHV chambers, as seen in the case of Zr on Cu(111). ZnO has a relatively low heat of formation (-83 kcal/mol), but the heats of formation of CeO_2 (-260 kcal/mol) and ZrO_2 (-262 kcal/mol) are very similar. The rapid reaction of the Zr atoms with O-containing molecules probably reflects a negligible stability of CuZr alloys when compared to a ZrO/Cu configuration. For the CeO_2/Cu(111) systems, the ceria islands acquired after dosing Ce on Cu(111) at 650K under an atmosphere of O_2 (5×10^{-7} Torr) exhibit sizes of in the range of 20-50 nm.[43] In the case of ZnO/Cu(111), the size of the oxide islands by depositing Zn in the same O_2 pressure at 550-600 K is in the range of 300-500 nm.[26] The relatively small island size seen for ZrO_2 on Cu(111), 10-12 nm, points to stronger oxide-metal interactions in the ZrO_2/Cu(111) system. These strong interactions probably prevent the formation of big islands of ZrO_2 and may play a role in the activation of CO_2 and its selective conversion to methanol.[18,24] Previous studies compared ZnO/Cu(111) and

CeO_x/Cu(111) with their conventional configuration Cu/ZnO(000$\bar{1}$) and Cu/CeO_2(111) respectively, and the oxide/metal arrangement led to a much higher methanol production rate from CO_2.[44] The special catalytic activity of such a configuration is probably the results of strong oxide-metal interaction, which lead to significant electronic perturbations in the oxides and to the novel chemical properties in consequence.[45] Therefore, a unique catalytic behavior for the ZrO_2/Cu(111) system may be expected.

4. Conclusion

The growth mode of low coverages (<0.2 ML) of zirconia in an inverse ZrO_2/CuO_x/Cu(111) configuration was investigated using STM and XPS. Two different preparation methods were applied to study their influence on the morphology and composition of the ZrO_2 nanoparticles formed. In the first method, the ZrO_2/CuO_x/Cu(111) model catalyst was prepared by two steps: (1) Zr was deposited on Cu(111) under UHV conditions, and (2) the Zr/Cu(111) surface was oxidized at 600 K. By this method, Zr and Cu(111) were oxidized at the same time, which leads to the intermixing of ZrO_2 and CuO_x. In the second method, the ZrO_2/CuO_x/Cu(111) surface was prepared in one step by directly depositing Zr under an O_2 ambient over a pre-oxidized CuO_x/Cu(111) surface, giving small ZrO_2 islands (~10 nm) with 2D structure. XPS proved the existence of ZrO_2(4+) by both methods; however, the oxidation of Zr/Cu(111) involved multiple species of Zr, due to the high reactivity of this metal under UHV conditions. Therefore, only the oxidative deposition was found to be a robust recipe to prepare ZrO_2/CuO_x/Cu(111) model catalysts. In addition, the thermostability of the ZrO_2/CuO_x/Cu(111) surface prepared by oxidative deposition was also investigated by annealing the surface up to 700 K in UHV. Neither the

morphology nor the oxidation state of ZrO_2 was affected under such annealing conditions, while the CuO_x was significantly reduced at elevated temperatures.

Acknowledgment

The research carried out at Brookhaven National Laboratory was supported by the U.S. Department of Energy, Office of Science and Office of Basic Energy Sciences under contract No. DE-SC0012704. SDS is supported by a U.S. DOE Early Career Award.

References

(1) Saeidi, S.; Amin, N. A. S.; Rahimpour, M. R. Hydrogenation of CO_2 to Value-Added Products—A Review and Potential Future Developments. *Journal of CO_2 Utilization* **2014**, *5*, 66–81.

(2) Quadrelli, R.; Peterson, S. The Energy–Climate Challenge: Recent Trends in CO_2 Emissions from Fuel Combustion. *Energy Policy* **2007**, *35* (11), 5938–5952.

(3) Tackett, B. M.; Gomez, E.; Chen, J. G. Net Reduction of CO_2 via Its Thermocatalytic and Electrocatalytic Transformation Reactions in Standard and Hybrid Processes. *Nature Catalysis* **2019**, 1.

(4) Wang, W.; Wang, S.; Ma, X.; Gong, J. Recent Advances in Catalytic Hydrogenation of Carbon Dioxide. *Chemical Society Reviews* **2011**, *40* (7), 3703.

(5) Olah, G. A. Beyond Oil and Gas: The Methanol Economy. *Angewandte Chemie International Edition* **2005**, *44* (18), 2636–2639.

(6) Goeppert, A.; Czaun, M.; Jones, J.-P.; Prakash, G. K. S.; A. Olah, G. Recycling of Carbon Dioxide to Methanol and Derived Products – Closing the Loop. *Chemical Society Reviews* **2014**, *43* (23), 7995–8048.

(7) Koitaya, T.; Yamamoto, S.; Shiozawa, Y.; Yoshikura, Y.; Hasegawa, M.; Tang, J.; Takeuchi, K.; Mukai, K.; Yoshimoto, S.; Matsuda, I.; et al. CO_2 Activation and Reaction on Zn-Deposited Cu Surfaces Studied by Ambient-Pressure X-Ray Photoelectron Spectroscopy. *ACS Catalysis* **2019**, *9* (5), 4539–4550.

(8) Rodriguez, J. A.; Liu, P.; Graciani, J.; Senanayake, S. D.; Grinter, D. C.; Stacchiola, D.; Hrbek, J.; Fernández-Sanz, J. Inverse Oxide/Metal Catalysts in Fundamental Studies and Practical Applications: A Perspective of Recent Developments. *The Journal of Physical Chemistry Letters* **2016**, *7* (13), 2627–2639.

(9) Saito, M.; Fujitani, T.; Takeuchi, M.; Watanabe, T. Development of Copper/Zinc Oxide-Based Multicomponent Catalysts for Methanol Synthesis from Carbon Dioxide and Hydrogen. *Applied Catalysis A: General* **1996**, *138* (2), 311–318.

(10) Nakamura, J.; Choi, Y.; Fujitani, T. On the Issue of the Active Site and the Role of ZnO in Cu/ZnO Methanol Synthesis Catalysts. *Topics in Catalysis* **2003**, *22* (3), 277–285.

(11) Behrens, M.; Studt, F.; Kasatkin, I.; Kühl, S.; Hävecker, M.; Abild-Pedersen, F.; Zander, S.; Girgsdies, F.; Kurr, P.; Kniep, B.-L.; et al. The Active Site of Methanol Synthesis over Cu/ZnO/Al_2O_3 Industrial Catalysts. *Science* **2012**, *336* (6083), 893–897.

(12) Lunkenbein, T.; Schumann, J.; Behrens, M.; Schlögl, R.; Willinger, M. G. Formation of a ZnO Overlayer in Industrial Cu/ZnO/Al_2O_3 Catalysts Induced by Strong Metal–Support Interactions. *Angewandte Chemie International Edition* **2015**, *54* (15), 4544–4548.

(13) Palomino, R. M.; Ramírez, P. J.; Liu, Z.; Hamlyn, R.; Waluyo, I.; Mahapatra, M.; Orozco, I.; Hunt, A.; Simonovis, J. P.; Senanayake, S. D.; et al. Hydrogenation of CO_2 on ZnO/Cu(100) and ZnO/Cu(111) Catalysts: Role of Copper Structure and Metal–Oxide Interface in Methanol Synthesis. *The Journal of Physical Chemistry B* **2018**, *122* (2), 794–800.

(14) Kattel, S.; Ramírez, P. J.; Chen, J. G.; Rodriguez, J. A.; Liu, P. Active Sites for CO_2 Hydrogenation to Methanol on Cu/ZnO Catalysts. *Science* **2017**, *355* (6331), 1296–1299.

(15) Samson, K.; Śliwa, M.; Socha, R. P.; Góra-Marek, K.; Mucha, D.; Rutkowska-Zbik, D.; Paul, J.-F.; Ruggiero-Mikołajczyk, M.; Grabowski, R.; Słoczyński, J. Influence of ZrO_2 Structure and Copper Electronic State on Activity of Cu/ZrO_2 Catalysts in Methanol Synthesis from CO_2. *ACS Catalysis* **2014**, *4* (10), 3730–3741.

(16) Wambach, J.; Baiker, A.; Wokaun, A. CO_2 Hydrogenation over Metal/Zirconia Catalysts. *Physical Chemistry Chemical Physics* **1999**, *1* (22), 5071–5080.

(17) Larmier, K.; Liao, W.-C.; Tada, S.; Lam, E.; Verel, R.; Bansode, A.; Urakawa, A.; Comas-Vives, A.; Copéret, C. CO_2-to-Methanol Hydrogenation on Zirconia-Supported Copper Nanoparticles: Reaction Intermediates and the Role of the Metal–Support Interface. *Angewandte Chemie International Edition* **2017**, *56* (9), 2318–2323.

(18) Tada, S.; Katagiri, A.; Kiyota, K.; Honma, T.; Kamei, H.; Nariyuki, A.; Uchida, S.; Satokawa, S. Cu Species Incorporated into Amorphous ZrO_2 with High Activity and Selectivity in CO_2 -to-Methanol Hydrogenation. *The Journal of Physical Chemistry C* **2018**, *122* (10), 5430–5442.

(19) Li, K.; Chen, J. G. CO_2 Hydrogenation to Methanol over ZrO_2-Containing Catalysts: Insights into ZrO_2 Induced Synergy. *ACS Catal.* **2019**, 7840–7861.

(20) Sato, A. G.; Volanti, D. P.; Meira, D. M.; Damyanova, S.; Longo, E.; Bueno, J. M. C. Effect of the ZrO_2 Phase on the Structure and Behavior of Supported Cu Catalysts for Ethanol Conversion. *Journal of Catalysis* **2013**, *307*, 1–17.

(21) Rhodes, M. D.; Bell, A. T. The Effects of Zirconia Morphology on Methanol Synthesis from CO and H_2 over Cu/ZrO_2 Catalysts: Part I. Steady-State Studies. *Journal of Catalysis* **2005**, *233* (1), 198–209.

(22) Witoon, T.; Chalorngtham, J.; Dumrongbunditkul, P.; Chareonpanich, M.; Limtrakul, J. CO_2 Hydrogenation to Methanol over Cu/ZrO_2 Catalysts: Effects of Zirconia Phases. *Chemical Engineering Journal* **2016**, *293*, 327–336.

(23) Gasser, D.; Baiker, A. Hydrogenation of Carbon Dioxide over Copper—Zirconia Catalysts Prepared by in-Situ Activation of Amorphous Copper—Zirconium Alloy. *Applied Catalysis* **1989**, *48* (2), 279–294.

(24) Kattel, S.; Yan, B.; Yang, Y.; Chen, J. G.; Liu, P. Optimizing Binding Energies of Key Intermediates for CO_2 Hydrogenation to Methanol over Oxide-Supported Copper. *J. Am. Chem. Soc.* **2016**, *138* (38), 12440–12450.

(25) Netzer, F. P.; Allegretti, F.; Surnev, S. Low-Dimensional Oxide Nanostructures on Metals: Hybrid Systems with Novel Properties. *Journal of Vacuum Science & Technology B* **2010**, *28* (1), 1–16.

(26) Mahapatra, M.; Kang, J.; Ramírez, P. J.; Hamlyn, R.; Rui, N.; Liu, Z.; Orozco, I.; Senanayake, S. D.; Rodriguez, J. A. Growth, Structure, and Catalytic Properties of ZnO_x Grown on CuO_x/Cu(111) Surfaces. *The Journal of Physical Chemistry C* **2018**, *122* (46), 26554–26562.

(27) Mahapatra, M.; Gutiérrez, R. A.; Kang, J.; Rui, N.; Hamlyn, R.; Liu, Z.; Orozco, I.; Ramírez, P. J.; Senanayake, S. D.; Rodriguez, J. A. The Behavior of Inverse Oxide/Metal Catalysts: CO Oxidation and Water-Gas Shift Reactions over ZnO/Cu(111) Surfaces. *Surface Science* **2019**, *681*, 116–121.

(28) Zhang, J.; Medlin, J. W. Catalyst Design Using an Inverse Strategy: From Mechanistic Studies on Inverted Model Catalysts to Applications of Oxide-Coated Metal Nanoparticles. *Surface Science Reports* **2018**, *73* (4), 117–152.

(29) Rodriguez, J. A.; Liu, P.; Graciani, J.; Senanayake, S. D.; Grinter, D. C.; Stacchiola, D.; Hrbek, J.; Fernández-Sanz, J. Inverse Oxide/Metal Catalysts in Fundamental Studies and Practical Applications: A Perspective of Recent Developments. *J. Phys. Chem. Lett.* **2016**, *7* (13), 2627–2639.

(30) Therrien, A. J.; Zhang, R.; Lucci, F. R.; Marcinkowski, M. D.; Hensley, A.; McEwen, J.-S.; Sykes, E. C. H. Structurally Accurate Model for the "29"-Structure of Cu_xO/Cu(111): A DFT and STM Study. *J. Phys. Chem. C* **2016**, *120* (20), 10879–10886.

(31) Matsumoto, T.; Bennett, R. A.; Stone, P.; Yamada, T.; Domen, K.; Bowker, M. Scanning Tunneling Microscopy Studies of Oxygen Adsorption on Cu(111). *Surface Science* **2001**, *471* (1), 225–245.

(32) Wiame, F.; Maurice, V.; Marcus, P. Initial Stages of Oxidation of Cu(111). *Surface Science* **2007**, *601* (5), 1193–1204.

(33) Lahtonen, K.; Lampimäki, M.; Hirsimäki, M.; Valden, M. Kinetic Hindrance during the Surface Oxidation of Cu(100)–c(10×2)-Ag. *The Journal of Chemical Physics* **2008**, *129* (19), 194707.

(34) Powell, C. X-Ray Photoelectron Spectroscopy Database XPS,Version 4.1, NIST Standard Reference Database 20, 1989.

(35) Paulidou, A.; M. Nix, R. Growth and Characterisation of Zirconia Surfaces on Cu(111). *Physical Chemistry Chemical Physics* **2005**, *7* (7), 1482–1489.

(36) Gondal, M.; Fasasi, T.; Baig, U.; Mekki, A. Effects of Oxidizing Media on the Composition, Morphology and Optical Properties of Colloidal Zirconium Oxide Nanoparticles Synthesized via Pulsed Laser Ablation in Liquid Technique. *Journal of Nanoscience and Nanotechnology* **2017**, *18*.

(37) Chase, M. W. NIST-JANAF Thermochemical Tables, 4th Edition. **1998**.

(38) Xue, M.; Nakayama, M.; Liu, P.; White, M. G. Electronic Interactions of Size-Selected Oxide Clusters on Metallic and Thin Film Oxide Supports. *J. Phys. Chem. C* **2017**, *121* (40), 22234–22247.

(39) Rameshan, C.; Li, H.; Anic, K.; Roiaz, M.; Pramhaas, V.; Rameshan, R.; Blume, R.; Hävecker, M.; Knudsen, J.; Knop-Gericke, A.; et al. In-Situ NAP-XPS Spectroscopy

during Methane Dry Reforming on ZrO_2/Pt(1 1 1) Inverse Model Catalyst. *Journal of Physics: Condensed Matter* **2018**, *30* (26), 264007.

(40) Orozco, I.; Huang, E.; Gutiérrez, R. A.; Liu, Z.; Zhang, F.; Mahapatra, M.; Kang, J.; Kersell, H.; Nemsak, S.; Ramírez, P. J.; et al. Hydroxylation of ZnO/Cu(111) Inverse Catalysts under Ambient Water Vapor and the Water–Gas Shift Reaction. *J. Phys. D: Appl. Phys.* **2019**, *52* (45), 454001.

(41) Lackner, P.; Choi, J. I. J.; Diebold, U.; Schmid, M. Substoichiometric Ultrathin Zirconia Films Cause Strong Metal–Support Interaction. *Journal of Materials Chemistry A* **2019**.

(42) Lang, N. D.; Yacoby, A.; Imry, Y. Theory of a Single-Atom Point Source for Electrons. *Physical Review Letters* **1989**, *63* (14), 1499–1502.

(43) Rodriguez, J. A.; Graciani, J.; Evans, J.; Park, J. B.; Yang, F.; Stacchiola, D.; Senanayake, S. D.; Ma, S.; Pérez, M.; Liu, P.; et al. Water-Gas Shift Reaction on a Highly Active Inverse CeO_x/Cu(111) Catalyst: Unique Role of Ceria Nanoparticles. *Angewandte Chemie International Edition* **2009**, *48* (43), 8047–8050.

(44) Senanayake, S. D.; Ramírez, P. J.; Waluyo, I.; Kundu, S.; Mudiyanselage, K.; Liu, Z.; Liu, Z.; Axnanda, S.; Stacchiola, D. J.; Evans, J.; et al. Hydrogenation of CO_2 to Methanol on CeO_x/Cu(111) and ZnO/Cu(111) Catalysts: Role of the Metal–Oxide Interface and Importance of Ce3+ Sites. *J. Phys. Chem. C* **2016**, *120* (3), 1778–1784.

(45) Rodriguez, J. A.; Liu, P.; Graciani, J.; Senanayake, S. D.; Grinter, D. C.; Stacchiola, D.; Hrbek, J.; Fernández-Sanz, J. Inverse Oxide/Metal Catalysts in Fundamental Studies and Practical Applications: A Perspective of Recent Developments. *The Journal of Physical Chemistry Letters* **2016**, *7* (13), 2627–2639.

TOC Graphic